

A novel Raman optical activity instrument operating in the deep ultraviolet spectral region

Josef Kapitán,^{a,b,*} Laurence D. Barron^a and Lutz Hecht^c

Raman optical activity (ROA) has been exclusively observed in the visible (VIS) and near-infrared (NIR) spectral regions to date. During the last few years, we have designed, constructed and tested the first ROA instrument, operating in the deep-ultraviolet (DUV) spectral region employing 244-nm excitation. This novel DUV ROA instrument is based on a backscattering geometry and incident circular polarization modulation (ICP); it makes use of a fast DUV imaging lens-based spectrograph and specially designed DUV grade polarization optics. The performance of this instrument has been evaluated by analysing measured non-resonant DUV ROA spectra of non-absorbing enantiomeric liquid samples and by comparing these with corresponding ROA spectra recorded in the visible spectral region. Copyright © 2015 John Wiley & Sons, Ltd.

Keywords: Raman optical activity; resonant Raman scattering; ultraviolet Raman optical activity

Introduction

Raman optical activity (ROA) typically refers to tiny intensity differences measured in Raman scattering from chiral molecules, either using right and left circularly polarized exciting radiation or analysing scattered Raman signals for right and left circular polarization states.^[1–5] These two different modulation strategies, respectively, measure incident circular polarization (ICP) and scattered circular polarization (SCP) forms of ROA. They originate in distinct time-even pseudoscalar molecular polarizability and optical activity tensor products and are virtually identical for non-absorbing molecules. ICP and SCP modulation consequently measure the same ROA spectra under non-resonant and otherwise comparable scattering conditions within the Rayleigh limit.^[3,4]

ROA exhibits an exquisite sensitivity for the identification of specific conformations and their changes, especially in biopolymers in aqueous solution, and frequently provides structural information not obtainable by other analytical techniques.^[6,7] However, ROA measurements, predominantly performed in the visible (VIS) spectral region, may still be occasionally plagued by annoying shortcomings, impeding a more widespread application of the technique particularly within a biochemical context.

The detection of VIS ROA spectra with an acceptable signal-to-noise ratio (SNR) may suffer from the application of rather high laser powers and relatively long acquisition and exposure times, may require the use of fairly large sample quantities and rather concentrated and pure samples and may frequently be hampered by either intensely coloured samples at non-transparent excitation wavelengths or strongly fluorescing trace impurities, potentially obscuring any Raman scattering due to comparatively much larger fluorescence cross sections and quantum yields.

To overcome these disadvantages, the measurement of ROA, employing other than the customary 488, 514.5 and 532-nm VIS excitations, have consequently been attempted or suggested.^[8,9] The use of longer excitation wavelengths offers the principal advantage of significantly suppressed fluorescent emission levels from impure or inherently fluorescing samples, and laser emission at 780 nm may be used routinely for the

excitation of ROA spectra.^[8] Suggestions to utilize 1064-nm excitation for the detection of Fourier transform ROA^[9] have never been realized in practice, presumably due to the lack of suitable detectors with sufficiently large quantum efficiencies and the significantly smaller scattering intensities in the near-infrared (NIR) region due to the dependences of Raman and ROA intensities on the frequency of the scattered radiation.^[1,8,10] Furthermore, NIR ROA does not appear to be viable for studies of biologically relevant molecules due to the associated poor signal-to-noise ratios (SNRs).

Intensity of Raman scattering is proportional to the fourth power of the wavenumber $\tilde{\nu}_s$ (or frequency) of the scattered radiation.^[10] On the other hand, ROA intensity is $\tilde{\nu}_s^5$ dependent due to the frequency dependence of the electric dipole-magnetic dipole optical activity tensor G' and the corresponding contribution from the electric dipole-electric quadrupole tensor A .^[1] Most modern spectroscopic detectors employed in the ultraviolet (UV), VIS and NIR spectral regions do not measure radiant flux (in Watts) directly; instead they operate in the photon counting regime. Since the relationship between photon flux P (number of photons per second) and radiant flux Φ is $P = \Phi/hc\tilde{\nu}_s$, the number of Raman and ROA scattered photons is proportional to $\tilde{\nu}_s^3$ and $\tilde{\nu}_s^4$, respectively.^[11]

The use of significantly shorter excitation wavelengths within the deep UV spectral region ($\lambda < 300$ nm) therefore holds great promise

* Correspondence to: Josef Kapitán, Department of Optics, Palacký University Olomouc, 17. listopadu 12, Olomouc 77146, Czech Republic.
E-mail: kapitán@optics.upol.cz

a Department of Chemistry, University of Glasgow, Joseph Black Building, Glasgow G12 8QQ, UK

b Department of Optics, Palacký University Olomouc, 17. listopadu 12, Olomouc 77146, Czech Republic

c Tracerco Technology Centre, Tracerco Ltd, Belasis Hall Business Park, Pavilion 10, The Moat, Billingham TS23 4ED, UK

for the acquisition of ROA spectra with significantly increased SNRs. On account of their large frequency dependence, considerably greater ROA intensities are predicted to occur within the DUV in comparison to other spectral regions. Depending on the detailed absorption characteristics of the sample under study, especially pre-, post- or rigorously resonant scattering conditions, DUV excitation is anticipated to generate Raman and ROA signal boosts of potentially several orders of magnitude.^[12,13] Significantly lower laser powers with smaller exposure and acquisition times may consequently be employed, and only relatively low sample concentrations may therefore be required for the measurement of DUV ROA spectra. Also, due to the relatively narrow spread of DUV Raman spectra and relatively large fluorescent Stokes shifts, excitations using sufficiently short wavelengths ($\lambda < 260$ nm) generally effect a virtually complete spectral separation of Raman and fluorescent emissions in condensed-phase samples.^[14–18] DUV Raman and ROA spectra are consequently not prone to SNR deteriorating interferences from fluorescent backgrounds so that sample purity may prove not to be such a critical factor for the detection of DUV ROA spectra. Depending on the extent of vibronic coupling, DUV ROA spectra of absorbing samples may, perhaps more importantly, provide a valuable source of novel structural information.

Despite these potential advantages of DUV ROA measurements, unfavourable scenarios have been identified which may considerably reduce the chances of DUV ROA detection or render it completely useless as a new source of structural information.^[19–23]

Similarly, anti-resonant scattering regimes with excitations approaching electronic transitions and causing largely reduced Raman and ROA intensities have been discussed.^[19–21] The ROA spectra of absorbing chiral molecules that show contributions predominantly from a single electronic state (SES) are predicted to exhibit a monosignate appearance with the sign of all bands being opposite to that of the single electronic transition's rotatory strength.^[22,23] On the other hand, any significant deviation of even monosignate resonant ROA relative intensities *versus* the parent

resonant Raman relative intensities is a breakdown of the SES limit and indicates the presence of intensity contributions of more than one excited electronic state.^[5]

To explore the practical feasibility of DUV ROA measurements the authors have designed, constructed and tested an appropriate ICP backscattering instrument, which is the subject of this paper.

Experimental

Samples

All chemicals were purchased from Sigma-Aldrich Corporation and used without any additional purification. Both enantiomers of menthol and borneol were dissolved in analytical grade CH_3OH , and those of glucose in distilled water. All the samples were studied in rectangular fused quartz microfluorescence cells with internal cross sections of 4×4 or 4×3 mm (Starna Scientific) in both the DUV and VIS ROA spectrometers.

Non-resonant VIS Raman and ROA spectra were measured employing a customized commercial ChiralRaman backscattering SCP instrument (BioTools Inc.) with 532-nm excitation and $\sim 7 \text{ cm}^{-1}$ spectral band-width.^[24] Non-resonant DUV Raman and ROA spectra were obtained using our newly constructed backscattering ICP instrument with 244-nm excitation and $\sim 15 \text{ cm}^{-1}$ spectral bandwidth.

Current experimental setup

The novel UV ROA spectrometer is based on a backscattering geometry and ICP modulation.^[25] This polarization modulation scheme has been selected mainly because of its relative simplicity, ease of implementation and the availability of suitable polarizing components functioning in the DUV spectral region. The layout of our new DUV ROA spectrometer is depicted schematically in Fig. 1. A continuous-wave intracavity frequency-doubled Ar^+ ion laser

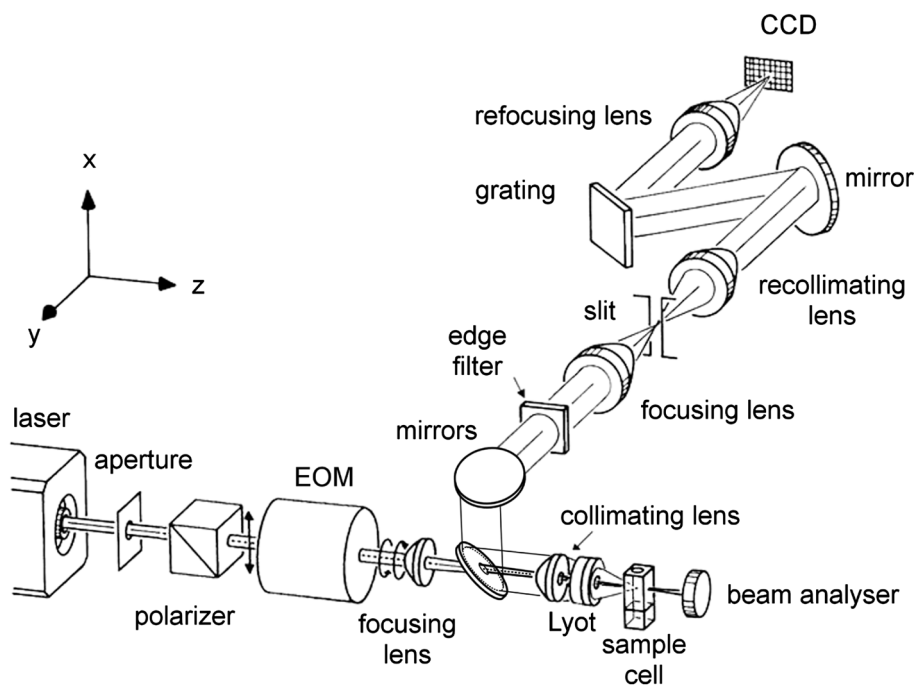


Figure 1. Schematic layout of the DUV ROA spectrometer. The spatial filter has been omitted for clarity (vide text for a more detailed description of individual optical components).

(Coherent, Model Innova 90C FRED) equipped with a β -barium borate frequency-doubling crystal for the generation of 244-nm DUV radiation is used as a radiation source.^[26]

Generating circularly polarized incident radiation

As in previous ROA instruments, an electro-optic modulator (EOM) was chosen to perform polarization modulation of the incident radiation between right and left circularly polarized states.^[25]

It is of paramount importance that high purity linearly polarized radiation enters the EOM. This task seems to be trivial, but selecting a high-quality polarizer has proven to be one of the main obstacles to the successful realization of our DUV ROA spectrometer. Several polarizers of different materials and several designs from various manufacturers have been tested, but a Glan-Taylor type polarizer made of the highest quality UV grade calcite (Bernhard Halle, model PGU12) has finally been implemented. Impurity free calcite is transparent above 220 nm. The above mentioned polarizer shows absorption losses <10% for 244-nm excitation radiation and an extinction ratio <10⁻⁶; it is also sufficiently stable in an incident laser beam of 1-mm waist diameter and radiant flux <10 mW. Linearly birefringent materials exist that are more transparent in the DUV region than calcite. However, we have found that, for example, α -barium borate (α -BBO) is not sufficiently stable (or our material has not been sufficiently pure); although crystal quartz and magnesium fluoride (MgF₂) are stable and transparent, they are much less birefringent than calcite, and a different type of polarizer (Rochon) has to be used with a potentially higher extinction ratio of 10⁻⁵. Crystal quartz is also circularly birefringent (optically active), which complicates polarization issues even further.

The DUV EOM is based on a longitudinal Pockels cell incorporating a potassium dideuterium phosphate (KD*P) crystal (Leysop, clear aperture 8 mm, in combination with a high voltage linear differential amplifier, model 5000) as in a previous VIS ROA spectrometer.^[25] KD*P is sufficiently transparent above 220 nm provided it does not contain residual impurities. Retardance of the Pockels cell is inversely proportional to wavelength, and hence the quarter-wave voltage is smaller in the DUV than in the VIS spectral region.

It has been necessary to develop a procedure for the fast and precise adjustment of the EOM in order to generate circularly polarized radiation with absolute values of ellipticities higher than 44° for successful DUV ROA measurements. The EOM crystal has to be precisely positioned (translation in *x* and *y* directions; rotations about *x*, *y* and *z* axes), and voltages for negative and positive quarter-wave retardation have to be accurately set. The *x* and *y* position of the incident laser beam within the EOM aperture is usually set prior to subsequent fine adjustments. However, five interdependent degrees of freedom remain. Several possible procedures exist for the setting of the EOM, but it was necessary to use one that avoids rotation of the EOM by a large angle and insertion of additional waveplates during or after the setup in order to eliminate the influence of other parameters on the final quality of the exiting polarized radiation. The polarization state of the emerging radiation has been tested by rotating a Glan-Taylor analyser (Thorlabs, model GL5) and by measuring its transmittance as a function of its rotation angle with a photodiode based power meter (Thorlabs, model S120V). This configuration is of course not able to distinguish between left- and right-elliptical polarization states; it measures merely the absolute value of the ellipticity, but its robustness and simplicity have proven to be a great advantage. The analyser is placed in a motorized rotation stage (Thorlabs model PRM1/MZ7)

and operated in step-scan mode synchronized with the EOM voltage switching and data readout from the power meter (Thorlabs, model PM100) connected to a PC via a RS232 interface. Since the GL5 polarizer operates outside its specified wavelength range, it exhibits solarization effects, namely increasing absorbance upon DUV irradiation (244 nm, > 2-mW laser power). These effects are fortunately reversible on a relatively short time scale of seconds, and continuous rotation of the analyser and placement of the laser beam outside the centre of the analyser aperture enable long-term and reproducible measurements. The quarter-wave voltage is switched alternately between positive-negative, negative-positive polarities etc. in order to exclude systematic offsets in radiant flux measurements for each voltage settings.

For perfectly circularly polarized radiation (exhibiting ellipticities $\chi \pm 45^\circ$) entering the rotating analyser, the output signal Φ_0 is independent of the analyser orientation. For general elliptically polarized radiation the output signal is a harmonic function from which the ellipticity can be calculated as $\chi = \arctan(\Phi_{0\min}/\Phi_{0\max})$, where $\Phi_{0\min}$ and $\Phi_{0\max}$ are the minimal and maximal values of the radiant flux detected during complete analyser rotation by 360°. Critical for a fast and correct EOM alignment is the observation that the power output signal for different voltages cross at certain 'nodes' and that these 'nodes' determine the best possible ellipticity achievable solely by voltage change; i.e. for situations when extremes of the output signal coincide with these nodes. Four nodes per rotation period of the analyser exist; two above and two below the constant line P_{conts} (see Fig. 2). Any two voltages are then sufficient for the identification of these 'nodes' and also for an estimate of the best possible ellipticity. The position of the nodes should be as close to the 'constant line' as possible, and it can be altered by fine rotation of the EOM crystal about the *x*, *y* and *z* axes. Rotations about different axes alter the position of the nodes in a different manner, so that the position of 'nodes' also determines the axis about which the rotation has to be performed in order to move the nodes close to the constant line. The laborious EOM alignment procedure was thus shortened from several hours to a simple reproducible routine lasting approximately 15 min, enabling frequent readjustments. The EOM needs to be readjusted every 2–3 days during measurements for successful recording of DUV ROA in order to maintain absolute value of ellipticities above 44°.

As in previously realized VIS ICP ROA instruments a combination of rotational and tilt stages for roll, pitch and yaw movements has been employed for the alignment of the EOM. Roll movement is achieved by a rotation stage (Newport, model M-UTR80SA), and since the rotation axis is aligned parallel to the crystal central axis, it virtually corresponds to a pure rotation about the *z* axis. Pitch movement is realized by a tilt stage (Newport, model M-TGN80) providing rotation about the *y* axis combined with translation along the +*x* and -*z* directions. Yaw movement is accomplished by another rotation stage (Newport, model M-UTR80SA), although the axis of rotation does not coincide with the crystal centre, so rotation about the *x* axis is also accompanied by translation along the -*y* direction. A representative example of the EOM alignment procedure is illustrated in Fig. 2.

Focusing circularly polarized incident radiation

The circularly polarized radiation emerging from the EOM is focused into the sample cell through holes drilled in a diverting mirror, collimating lens and Lyot depolarizer (Fig. 1).^[25] The beam waist

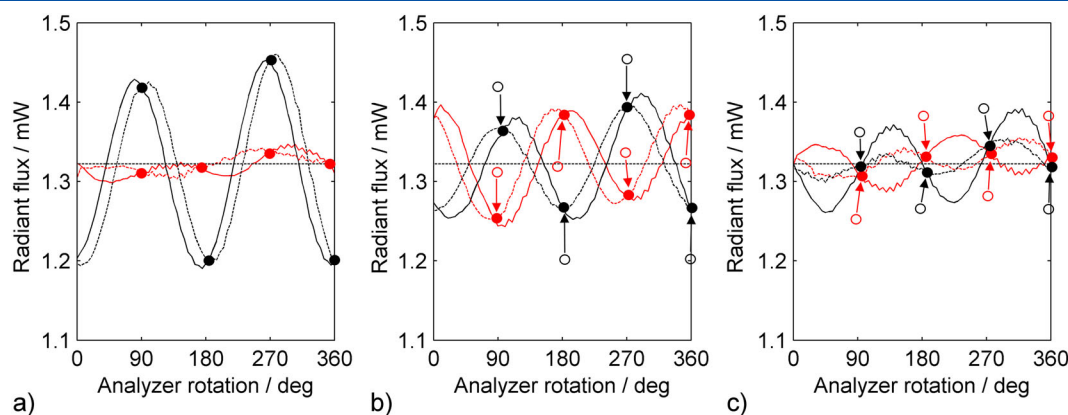


Figure 2. Detection of ellipticity in the excitation beam emerging from the EOM. Each panel contains four measurements; positive (red) and negative (black) voltages of two different values (solid and dashed curves). Positions of nodes are marked by solid circles, positions of nodes from previous steps are marked by empty circles and arrows indicate changes in node position compared to previous steps. a) Initial measurement: positive voltage generates virtually perfectly circularly polarized radiation (ellipticity 44.1°), but negative voltage generates elliptically polarized radiation with ellipticity 39.3° . b) Changes after EOM rotation about the z axis by 1.3° : node pairs (above each other) move in the same direction. c) Changes after pitch movements consisting of a rotation about the y axis by 0.6 mrad, a translation along the z axis by -0.06 mm and translation along the x axis by 0.05 mm. Absolute values of ellipticities measured after these fine adjustments are 43.9° and 43.8° for positive and negative voltages, respectively. The voltages are subsequently finely tuned in order to move the curve maxima to nodes (not shown), thereby achieving an absolute value of ellipticity of more than 44.1° for both arms. This figure is available in colour online at wileyonlinelibrary.com/journal/jrs

diameter in the focal region should be approximately $25\ \mu\text{m}$ in order not to overfill the spectrograph entrance slit with a width of $25\text{--}50\ \mu\text{m}$ too much (taking into account aberrations and close to unit magnification of the collection optics). Since a free working distance of at least 15 cm is needed because of the physical dimensions of the depolarizing and collecting optics and the diverting mirror, the laser beam diameter has to be expanded twofold prior to focusing in order to achieve the desired beam waist diameter in the focal region. The beam expander is realized by two best form lenses of focal lengths 50 mm and 100 mm (CVI) and a $50\text{-}\mu\text{m}$ diameter pinhole is placed in their common focus, so that the beam expander works also as a spatial filter. The spatial filter unit significantly enhances the quality of the incident laser beam and makes it less prone to contamination by scattering particles that are inevitably attracted to optical element surfaces due to an optical tweezers effect. The expanded beam is subsequently focused by another $f=200$ -mm best form lens. All lenses are made from fused silica; they are stress free and do consequently not affect the polarization state of the incident radiation due to any residual linear birefringence.

For measurements with a wider slit ($50\ \mu\text{m}$), a larger beam waist diameter of $50\ \mu\text{m}$ is used. In this case the spatial filter consists of two $f=50$ -mm best form lenses, so that the diameter of the laser beam remains unchanged, and unit magnification is maintained. In principle the entire unit may have been omitted. Nevertheless, the benefits of the spatial filter, significantly improving the laser beam quality, more than justify the filter's presence.

Depolarizing, collecting and analysing Raman scattered radiation

Mirrors and especially diffraction gratings represent polarizing elements. It was relatively early recognized that in order to accomplish successful ICP ROA measurements in backscattering, a Lyot depolarizer is a critical optical element which has to be placed in the diverging beam of the backscattered Raman radiation.^[27] Initially a Lyot depolarizer made from quartz (Leysop, custom made model, total length of 20 mm) consisting of three plates of thicknesses in the ratio $2:1:4$ has been tested. However, we were unable to find the optimum rotation (about the z-axis) in order

to achieve a sufficiently low level of polarization artefacts. Quartz has been selected because of its high DUV transmittance, but its circular birefringence is probably the main reason for its failure. A much thinner depolarizer made of UV grade calcite with two plates of thickness 4 and 2 mm with a 20×20 mm octagonal aperture, cemented with UV transparent cement (manufactured by Bernhard Halle GmbH.) has subsequently been tested. A small 1 -mm hole has been drilled through the Lyot depolarizer. This Lyot depolarizer is sufficiently transparent, and its much lower thickness causes also smaller spherical aberration due to its presence in a divergent beam.

The divergent beam of backscattered Raman radiation is collimated by a plano-convex lens of focal length 36 mm and aperture diameter 25 mm (CVI, model PLCX-25.4-18.0-UV-248-355). The quasi-collimated beam is subsequently diverted by a pair of 2 -inch diameter circular mirrors with two narrow band dielectric coatings (CVI, model TLM1) within a 'polarization neutral' arrangement (see Fig. 1).^[28] This utilization of two mirrors is in practice not necessary, but it provides more flexibility in aligning the train of optical elements. Rayleigh scattering in the diverted beam is subsequently efficiently suppressed by an edge filter (Materion, model with OD5 at 244 nm, edge slope <4 nm) and focused onto the spectrograph entrance slit by a $f/2$ plano-convex lens with a focal length of 25 mm (CVI, model PLCX-25.4-12.9-UV-248-355). This particular optical system exhibits a relatively large amount of spherical and chromatic aberrations, because of the use of singlet plano-convex lenses and the introduction of flat optical elements into a diverging beam (cell window, Lyot depolarizer). Custom made achromatized aspherical doublet lenses will be used in future versions of the spectrometer in order to correct for these aberrations.

Spectral analysis and data recording are performed by a home designed deep DUV lens-based imaging spectrograph with a large $f/2$ aperture, equipped with a reflective grating with 3600 grooves mm^{-1} operating at first order, a silicon deep depletion CCD detector (Renishaw plc, Model UV-RenCam) and the data collection being synchronized with ICP modulation.^[26] The DUV spectrograph and its detection system are described in detail elsewhere,^[26] the only difference being that the individual elements of the compound focusing and collimating lenses inside

the spectrograph have been anti-reflection coated for a spectral range of 225–308 nm (coating provided by CVI) that significantly increased the transmittance of the entire system.

Backscattered DUV Raman intensities

Raman and ROA intensities measured with the DUV ROA instrument employing 244-nm excitation will be compared with data recorded using a commercial VIS ROA instrument with 532-nm excitation (Biotools, ChiralRaman) described in detail elsewhere.^[24]

In order to compare Raman spectra measured with two distinct spectrographs operating in very different spectral regions (DUV and VIS), the data must be evaluated using identical units. Detected signals strengths are usually expressed in ADC counts which may be converted into electronic charge (e^-) units by multiplication with the reciprocal gain of the CCD camera system, which results in 2.5 and 8 e^- per ADC count for the DUV^[23] and VIS system respectively; it is customary to display the Raman intensity scale in the e^- units. Spectral intensities ought to be scaled by the number of electronic charges per detector element (pixel). However, this value is not a good measure, since the spectral width of a pixel may vary not only between different spectrographs, but also within the same spectrum (see Fig. 3a), and the information about the pixel spectral width may not always be specified. We will therefore compare measured intensities in e^-/cm^{-1} ($e^- \times \text{cm}$) units, as the number of detected electrons per pixel is divided by the pixel spectral width. This fact has to be taken into account when integral peak intensities are calculated.

Raman spectra in the DUV and VIS spectral regions are measured with different acquisition times and excitation laser powers. A much higher radiant flux can be used in the VIS spectral region without any danger of sample photo-degradation. It is thus suitable to compare intensities per unit excitation energy ($e^- \times \text{cm} \times \text{J}^{-1}$).^[28] As mentioned in the introduction, Raman scattering intensities depend on the third power of wavenumber of the scattered radiation $\tilde{\nu}_s$, for photon counting detectors (in case the irradiance of the exciting radiation is expressed in W/m^2). Measured signals for different excitation wavelengths may therefore be only directly compared if the correction for this dependence is taken into account (see Figs. 3b, 4) so that the resulting unit for the detected signal reads $e^- \times \text{cm}^4 \times \text{J}^{-1}$. However, the difference in the wavenumber-dependent correction factor varies by only approximately 20% within the selected wavenumber range 0–2000 cm^{-1} and can consequently be safely neglected in most cases (as in Figs. 5–7).

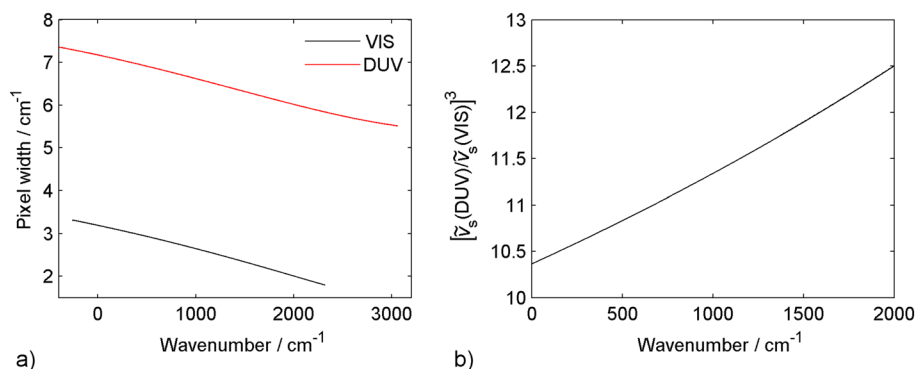


Figure 3. a) Pixel spectral widths for the VIS (black) and DUV (red) ROA spectrometers. b) Ratio of third-power wavenumber dependence of Raman scattering for UV and VIS Raman spectrometers with excitation wavelengths of 244 and 532 nm in the photon counting regime. This figure is available in colour online at wileyonlinelibrary.com/journal/jrs

As is evident from the comparison of Raman spectra displayed in Fig. 4 the DUV Raman intensities are more than three orders of magnitude smaller than anticipated for the case of equally efficient DUV and VIS Raman scattering collection and detection systems. However, the efficiency and transmittance values of the DUV ROA spectrometer components are generally significantly smaller than those of the VIS ROA spectrometer (Table 1), which may easily explain the efficiency difference of approximately two orders of magnitude, with a much lower efficiency of the DUV CCD detector being the most important factor. The VIS ROA spectrometer also exhibits an efficient cross-section transformer^[28] with an effective large circular aperture of diameter more than 1.5 mm being utilized at the entrance of the spectrograph. In contrast, a narrow entrance slit of 25 μm is employed in the DUV ROA spectrograph. The slit height is 6 mm, but only the central part (~ 1 mm) is effectively used. The DUV ROA spectrometer is also impaired by larger aberrations in the light collection optics, so that an overall remaining factor of ten from the signal comparison may be easily attributed to these effects. It should also be mentioned that the spectral resolution of the DUV spectrometer is approximately two times worse than that for the VIS spectrometer.

DUV ROA backscattering spectra

Tests for the correct functioning of the ROA spectrometer are conducted within a non-resonant scattering regime so that any potential complications associated with pre-, post or rigorous resonant scattering scenarios may be safely avoided. Since they do not possess any chromophores, which might absorb the exciting or scattered radiation in the DUV or VIS spectral regions, and since their VIS ROA spectra have already been recorded and both enantiomers of each are readily available, menthol,^[29–31] borneol^[32] and glucose^[33] have been selected as ideal candidates for this initial DUV ROA study.

Results and discussion

The DUV ICP and VIS SCP Raman and ROA spectra of all the samples (Figs. 5–7) were measured at ambient temperature and are presented as raw circular intensity sums ($I^R + I^L$) and ($I_R + I_L$), and circular intensity differences ($I^R - I^L$) and ($I_R - I_L$), respectively. I^R and I^L denote the Raman intensities using right and left circularly polarized incident radiation; whereas I_R and I_L are the intensities of right and left circularly polarized Raman-scattered radiation.

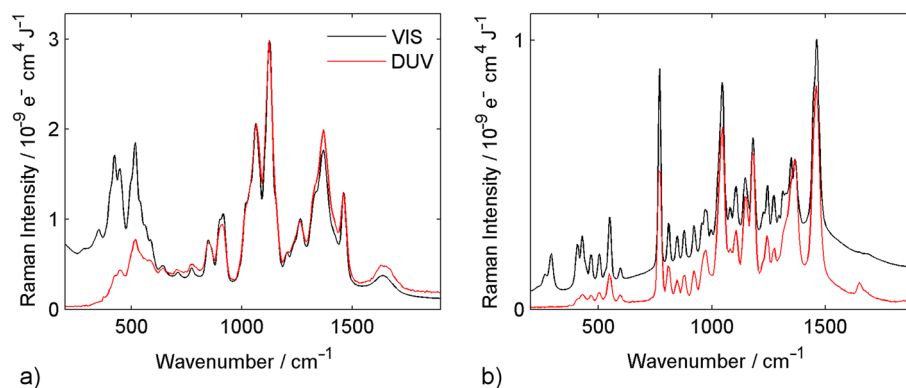


Figure 4. Comparison of Raman spectra of a) a 3 mol/l aqueous solution of D-glucose and b) solution of (–)-Menthol (2.6 g in 1.0-g methanol) recorded with VIS (black) and DUV (red) ROA spectrometers. The VIS Raman spectra intensity has been divided by an empirical factor of 1400 in order to display spectra onto the same intensity scale. The cutoff wavenumber for the DUV edge filter is approximately 450 cm^{-1} . Laser powers measured at the sample for the DUV spectra are 2.7 mW; those for VIS spectra are 270 mW (glucose) and 40 mW (menthol). Accumulation times for the DUV spectra are 40 s; those for VIS spectra are 1560 s (glucose, scaled to ~ 1.1 s) and 1410 s (menthol, scaled to ~ 1.0 s). All spectra have been corrected for spectral pixel width (cm^{-1}), excitation energy (J) and ν_s dependence (cm^{-3}). This figure is available in colour online at wileyonlinelibrary.com/journal/jrs

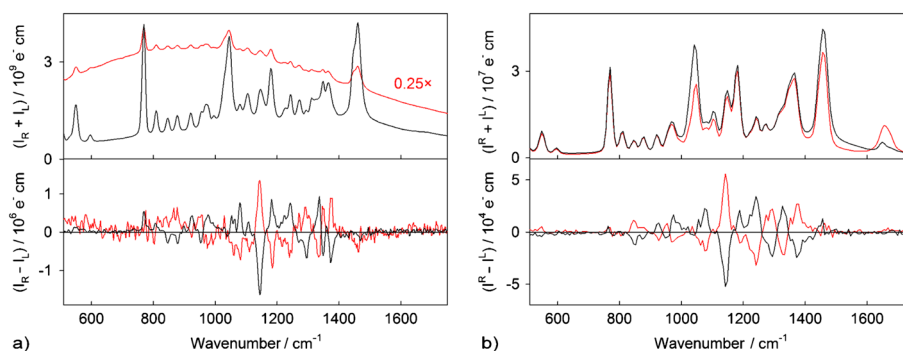


Figure 5. Non-resonant backscattering Raman (top) and ROA (bottom) spectra of (+)-menthol (red) and (–)-menthol (black) solution (2.3 g in 1.0 g methanol) with a) 532-nm excitation, SCP modulation, accumulation time 0.61 h (+), 0.39 h (–), laser power measured at the sample 25 mW (+), 40 mW (–) and b) 244-nm excitation, ICP modulation, accumulation time 15 h and laser power 3 mW for both (+) and (–). The VIS Raman spectrum of (+)-menthol has been reduced by a factor of four due to strong sample fluorescence. This figure is available in colour online at wileyonlinelibrary.com/journal/jrs

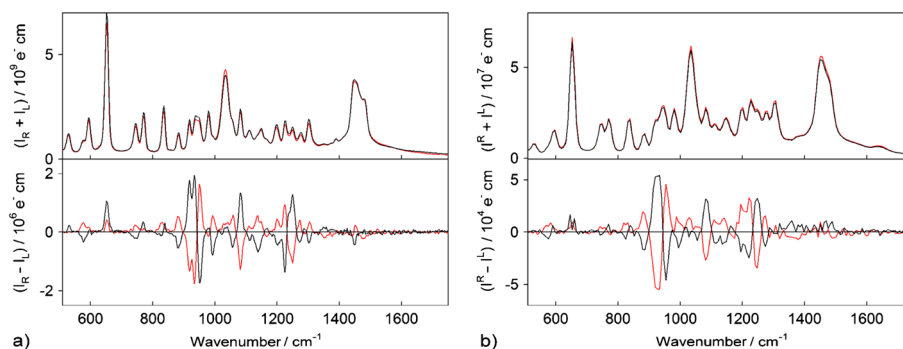


Figure 6. Non-resonant backscattering Raman (top) and ROA (bottom) spectra of (+)-borneol (red) and (–)-borneol (black) solution (1.0 g in 1.0-g methanol) with a) 532-nm excitation, SCP modulation, accumulation time 0.37 h, laser power measured at the sample 80 mW and b) 244-nm excitation, ICP modulation, accumulation time 28 h and laser power 3 mW. This figure is available in colour online at wileyonlinelibrary.com/journal/jrs

All of our commercially available samples have intentionally not been recrystallized to remove any potential mildly fluorescing impurities. The VIS Raman spectrum of naturally occurring (–)-menthol (Fig. 5a) exhibits only residual fluorescence emission levels, whereas that of the synthetic (+)-menthol and to a lesser extent also that of D-glucose (Fig. 7a) suffer from a noticeable fluorescence background. However, due to the superior performance of the commercial VIS SCP ROA instrument, and apart from a noticeable signal-to-noise degradation, the presence of

fluorescence does not introduce any major artefacts or distortions into the measured VIS ROA spectrum of contaminated (+)-menthol. The VIS ROA spectra of both enantiomers of all the studied molecules still display virtually perfect mirror image symmetry in the wavenumber region $\sim 800\text{--}1400\text{ cm}^{-1}$.

Although the DUV Raman spectra have been measured with noticeably lower spectral resolution than the corresponding VIS Raman spectra, they do in contrast not show any sign of fluorescence contamination. Presumably due to fluorescence mediated

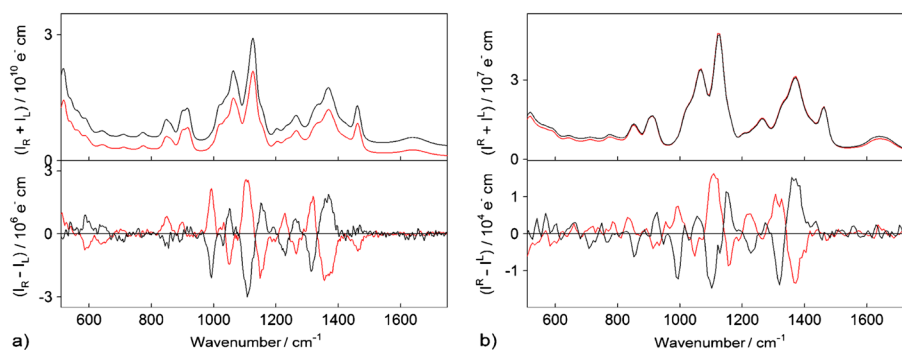


Figure 7. Non-resonant backscattering Raman (top) and ROA (bottom) spectra of L- (red) and D-glucose (black) solution in water (3 mol/l) with a) 532-nm excitation, SCP modulation, accumulation time 1.0 h, laser power measured at the sample 240 mW and b) 244-nm excitation, ICP modulation, accumulation time 57 h and laser power 3 mW. All spectra were subjected to mild third-order five point Savitzky–Golay smoothing. This figure is available in colour online at wileyonlinelibrary.com/journal/jrs

Table 1. Comparison of diffraction efficiency, transmittance and reflection of optical elements implemented in the VIS and DUV ROA spectrometers. Polarization optics implemented in the scattered beam comprise of retardation plates, a liquid crystal retarder and polarization beam-splitters in the VIS and a Lyot depolarizer in the DUV ROA spectrometer

Spectrometer element efficiency	DUV (%)	VIS (%)	Factor VIS/DUV
CCD	10	80	8
Diffraction grating	40	80	2
Lenses	50	90	1.8
Mirror, vignetting	70	95	1.4
Edge/notch filter	60	90	1.5
Polarization optics	50	70	1.4
Total:			90

Table 2. Comparison of selected CID ratios of DUV and VIS CIDs of (–)-menthol

Band position/cm ⁻¹	DUV × 10 ³	VIS × 10 ⁴	DUV/VIS
847	–2.6	–4.2	6.2
877	–1.0	–3.6	2.8
926	2.2	8.2	2.7
954	–0.6	–3.0	2.0
972	1.7	4.5	3.8
1225	3.0	6.7	4.4
1242	3.4	6.9	4.9
1272	–1.1	–2.8	3.9
1293	–4.1	–12.2	3.4

oxidative photon damage, some of the DUV Raman bands of contaminated (+)-menthol but particularly the two strongly polarized bands observed at ~ 1045 and ~ 1458 cm⁻¹ exhibit significantly lower intensities than the equivalent DUV Raman band intensities of less contaminated (–)-menthol (Fig. 5b) and a much higher intensity of the ~ 1650 cm⁻¹ band. However, the DUV ICP ROA spectra of both enantiomers show almost perfect mirror-image symmetry in the wavenumber region ~ 800 – 1450 cm⁻¹. They also exhibit slightly better SNRs than the corresponding VIS SCP ROA spectra and, accounting for the different spectral resolutions and the non-ideal transmission characteristics of the utilized DUV edge filter,^[26] are virtually identical to the VIS SCP ROA spectra, confirming the validity of the simplifying approximations associated with the non-resonant ROA scattering regimes.

A direct comparison of Raman and ROA intensities measured using the DUV ICP and VIS SCP ROA instruments is not easily performed due to the very different characteristics of the two instruments and the significantly larger spectral bandwidth employed for the detection of DUV spectra. However, the ratios of the ROA and Raman band intensities referred to as normalized circular intensity differences (CIDs) do not depend on instrumental response.^[1] Consequently, on account of the linear frequency dependence of the G' tensor and the corresponding contribution from the A tensor,^[1] the ratio of the DUV and VIS CIDs for individual bands should be given by the ratio of the corresponding DUV and VIS wavenumbers (or frequencies) $\tilde{\nu}_s(\text{DUV})/\tilde{\nu}_s(\text{VIS})$ of scattered radiation.

Those Raman bands of the less contaminated (–)-menthol which do not overlap with any solvent Raman bands have been analysed (Table 2) in detail. It is evident that the selected CID ratios are larger than the reference value ≈ 2.2 – 2.5 . However, the error in determination of the CIDs is relatively high and is strongly influenced by the magnitude of the Raman spectral backgrounds.

For quantitative discussion of SNRs in DUV and VIS ROA spectra, it is assumed, that the major contribution to noise is statistical (shot) noise. The Raman scattering signal associated with left and right circularly polarized radiation may be expressed as $I = qN \approx I(R) \approx I(L)$, where N is a number of scattered photons and q is a positive factor smaller than one corresponding to the efficiency of the spectrometer and detector. ROA signals may be expressed as $I(R) - I(L) \approx \text{CID} \times 2I$, the corresponding (statistical) noise as $\sqrt{2I}$ and ROA SNRs as $\text{CID} \sqrt{qN}/2$. Since $\text{CID}_{\text{DUV}}/\text{CID}_{\text{VIS}} \approx \tilde{\nu}_s(\text{DUV})/\tilde{\nu}_s(\text{VIS})$, $N_{\text{DUV}}/N_{\text{VIS}} \approx \tilde{\nu}_s^3(\text{DUV})/\tilde{\nu}_s^3(\text{VIS})$ and the ratio of spectrometer efficiencies estimated from the intensities of corresponding Raman spectra is $q_{\text{DUV}}/q_{\text{VIS}} \approx 1/1400$ (Fig. 4), the predicted ratio of signal-to-noise ratios is $\text{SNR}_{\text{DUV}}/\text{SNR}_{\text{VIS}} \approx 0.2$.

ROA spectra of non-fluorescing samples of menthol (Fig. 5) and borneol (Fig. 6) have approximately similar SNRs, but the excitation energy (the accumulation time multiplied by the laser power) is approximately three times larger for the DUV than for the VIS spectra. Similarly, the DUV ROA spectrum of glucose (Fig. 7) exhibits SNR approximately three times smaller than corresponding VIS ROA spectrum of glucose, but the excitation energy in both cases is approximately same. Consequently, it can be estimated from our data, that $\text{SNR}_{\text{DUV}}/\text{SNR}_{\text{VIS}} \approx 0.3$. Within experimental errors this result

is thus in agreement with the predicted value 0.2. The observed difference may easily be attributed to a lower resolution and hence higher relative signals of the DUV spectra.

Conclusions

A ROA spectrometer for the DUV spectral region has been successfully realized for the first time. Its construction has proved to be significantly more challenging than that of VIS ROA instruments due to the great difficulties associated with generating and manipulating polarized DUV radiation. However, a procedure for the fast and reliable EOM alignment has been developed for the generation of high purity circularly polarized DUV radiation, and polarization artefacts were successfully minimized by employing a Lyot depolarizer in the diverging beam of the scattered Raman radiation. DUV ROA spectra of several enantiomeric samples in aqueous and non-aqueous solutions have been measured, which prove to be of high quality. Non-resonant spectra may be recorded more easily and in a shorter time with our VIS ROA spectrometer predominantly because the advantage of greater DUV Raman and ROA intensities is largely negated by the necessity for using a much lower laser power and a worse performance and efficiency of the optical system for the collection and detection of DUV radiation. However, the situation may be dramatically different in pre-resonant or rigorously resonant scattering regimes, which may prove to be the main application for the new DUV ROA spectrometer, as will be reported in our subsequent publications. We have also demonstrated that DUV Raman spectra are generally not plagued by any residual fluorescence, which may be a decisive advantage for the study of auto-fluorescing samples. The design of the collection optics and especially the efficiency of detectors may admittedly be significantly improved. Nevertheless, we think that our construction of the first DUV ROA spectrometer represents an important milestone in the exploration of pre-resonant and rigorously resonant Raman and ROA scattering phenomena of a wide range of biologically interesting molecules.

Acknowledgements

This work is supported by grants from the UK Engineering and Physical Sciences Research Council and Technology Agency of the Czech Republic (project no. TE01020229). We would also like to thank Götz Zinner from Bernhard Halle and Steve Payne from Leysop for their help in the development of custom made optics.

References

- [1] L. D. Barron, *Molecular Light Scattering and Optical Activity*, 2nd ed., Cambridge University Press, Cambridge, **2004**.
- [2] L. D. Barron, A. D. Buckingham, *Chem. Phys. Lett.* **2010**, *492*, 199.
- [3] L. D. Barron, J. R. Escribano, *Chem. Phys.* **1985**, *98*, 437.
- [4] L. A. Nafie, in *Encycl. Spectrosc. Spectrom.* (Eds.: J. Lindon, G.E. Tranter, D.W. Koppenaal), Academic Press, Oxford, **2010**, pp. 2397–2405.
- [5] L. A. Nafie, *Vibrational Optical Activity: Principles and Applications*, John Wiley & Sons, Chichester, **2011**.
- [6] L. D. Barron, *Curr. Opin. Struct. Biol.* **2006**, *16*, 638.
- [7] L. D. Barron, L. Hecht, in *Compr. Chiroptical Spectrosc.* Vol 2 (Eds.: N. Berova, P.L. Polavarapu, K. Nakanishi, R.W. Woody), John Wiley & Sons, Inc., Hoboken, New Jersey, **2012**, pp. 759–793.
- [8] L. A. Nafie, B. E. Brinson, X. Cao, D. A. Rice, O. M. Rahim, R. K. Dukor, N. J. Halas, *Appl. Spectrosc.* **2007**, *61*, 1103.
- [9] P. L. Polavarapu, *Chem. Phys. Lett.* **1988**, *148*, 21.
- [10] D. A. Long, *The Raman Effect: A Unified Treatment of the Theory of Raman Scattering by Molecules*, John Wiley & Sons, Chichester, **2002**.
- [11] R. L. McCreery, *Raman Spectroscopy for Chemical Analysis*, John Wiley & Sons, Chichester, **2000**.
- [12] K. H. Fung, I. N. Tang, *Appl. Spectrosc.* **1992**, *46*, 159.
- [13] B. Küstner, C. Schmuck, P. Wich, C. Jehn, S. K. Srivastava, S. Schlücker, *Phys. Chem. Chem. Phys.* **2007**, *9*, 4598.
- [14] S. A. Asher, C. R. Johnson, *Science* **1984**, *225*, 311.
- [15] S. A. Asher, *Anal. Chem.* **1993**, *65*, 59A.
- [16] L. C. T. Shoute, K. J. Schmidt, R. H. Hall, M. A. Webb, S. Rifai, P. Abel, P. H. Arboleda, A. Savage, J. T. Bulmer, G. R. Loppnow, *Appl. Spectrosc.* **2002**, *56*, 1308.
- [17] G. R. Loppnow, L. Shoute, K. J. Schmidt, A. Savage, R. H. Hall, J. T. Bulmer, *Philos. Trans. R. Soc. -Math. Phys. Eng. Sci.* **2004**, *362*, 2461.
- [18] D. D. Tuschel, A. V. Mikhonin, B. E. Lemoff, S. A. Asher, *Appl. Spectrosc.* **2010**, *64*, 425.
- [19] S. Hassing, *J. Raman Spectrosc.* **1997**, *28*, 739.
- [20] R.-H. Zheng, W.-M. Wei, *J. Phys. Chem. A* **2007**, *111*, 3652.
- [21] S. Lubner, J. Neugebauer, M. Reiher, *J. Chem. Phys.* **2010**, *132*. DOI:10.1063/1.3300069.
- [22] L. A. Nafie, *Chem. Phys.* **1996**, *205*, 309.
- [23] L. A. Nafie *Theor. Chem. Acc.* **2008**, *119*, 39.
- [24] L. D. Barron, F. Zhu, L. Hecht, G. E. Tranter, N. W. Isaacs, *J. Mol. Struct.* **2007**, *834–836*, 7.
- [25] L. Hecht, L. D. Barron, E. W. Blanch, A. F. Bell, L. A. Day, *J. Raman Spectrosc.* **1999**, *30*, 815.
- [26] L. Hecht, J. Clarkson, B. J. E. Smith, R. Springett, *J. Raman Spectrosc.* **2006**, *37*, 562.
- [27] W. Hug, in *Raman Spectrosc.* (Eds.: J. Lascombe, P.V. Huong), Wiley-Heyden, Chichester, **1982**, pp. 3–12.
- [28] W. Hug, G. Hangartner, *J. Raman Spectrosc.* **1999**, *30*, 841.
- [29] M. Baranska, K. Chruszcz-Lipska, *Nat. Prod. Commun.* **2010**, *5*, 1417.
- [30] L. D. Barron, B. P. Clark, *J. Chem. Soc. Perkin Trans. 2* **1979**, 1164.
- [31] L. D. Barron, L. Hecht, S. M. Blyth, *Spectrochim. Acta Part Mol. Spectrosc.* **1989**, *45*, 375.
- [32] L. D. Barron, *J. Chem. Soc.-Perkin Trans. 2* **1977**, 1074.
- [33] Z. Q. Wen, L. D. Barron, L. Hecht, *J. Am. Chem. Soc.* **1993**, *115*, 285.